

## In-plane uniaxial magnetic anisotropy in epitaxial Fe<sub>3</sub>O<sub>4</sub>-based hybrid structures on GaAs(100)

W. Zhang,<sup>1</sup> J. Z. Zhang,<sup>2</sup> P. K. J. Wong,<sup>3</sup> Z. C. Huang,<sup>1,2</sup> L. Sun,<sup>2</sup> J. L. Liao,<sup>1</sup> Y. Zhai,<sup>2,4</sup> Y. B. Xu,<sup>1,5,\*</sup> and G. van der Laan<sup>6</sup>

<sup>1</sup>*Spintronics and Nanodevice Laboratory, Department of Electronics, University of York, York YO10 5DD, United Kingdom*

<sup>2</sup>*Department of Physics, Southeast University, Nanjing 211189, China*

<sup>3</sup>*NanoElectronics Group, MESA+ Institute of Nanotechnology, University of Twente, P.O. Box 217, 7500 AE Enschede, the Netherlands*

<sup>4</sup>*National Laboratory of Solid Microstructure, Center for Analysis, Nanjing 210093, China*

<sup>5</sup>*Nanjing-York Joint Center in Spintronics (NYCS), Nanjing University, Nanjing 210006, China*

<sup>6</sup>*Diamond Light Source, Chilton, Didcot OX11 0DE, United Kingdom*

(Received 15 June 2010; revised manuscript received 5 July 2011; published 30 September 2011)

The evolution of the in-plane magnetic anisotropies in Fe<sub>3</sub>O<sub>4</sub>/GaAs(100) and Fe<sub>3</sub>O<sub>4</sub>/MgO/GaAs(100) hybrid spintronic structures has been studied by magneto-optical Kerr effect and ferromagnetic resonance (FMR). The surface and volume contributions to the in-plane cubic and uniaxial anisotropies have been distinguished in Fe<sub>3</sub>O<sub>4</sub>/GaAs by fitting the anisotropy constants, measured by FMR, as a function of the magnetic film thickness. It was found that interfacial chemical bonding rather than strain relaxation plays the dominant role in causing the unexpected uniaxial magnetic anisotropy (UMA) in Fe<sub>3</sub>O<sub>4</sub> films grown directly on the GaAs surfaces. In contrast, after MgO barrier insertion, FMR results show that the UMA is greatly reduced, and strain relaxation is found to be the main origin of the UMA in Fe<sub>3</sub>O<sub>4</sub>/MgO/GaAs structures.

DOI: [10.1103/PhysRevB.84.104451](https://doi.org/10.1103/PhysRevB.84.104451)

PACS number(s): 75.70.-i, 85.75.-d

### I. INTRODUCTION

The combination of strongly spin-polarized materials and semiconductors to form hybrid magnetic/semiconductor structures constitutes the core of semiconductor spintronics, which is aimed at straightforward integration with current magnetic technologies in microelectronics.<sup>1</sup> An obvious advantage of linking spintronic materials with III-V semiconductors is the benefit of utilizing materials widely employed in the microelectronics industry; i.e., such systems are well understood and enable integration with existing technologies.<sup>2</sup> One particularly interesting candidate for room-temperature spintronic applications is half-metallic Fe<sub>3</sub>O<sub>4</sub> (magnetite), which at room temperature is ferrimagnetic with a high Curie temperature,  $T_C = 858$  K.<sup>3</sup> The strong spin polarization near the Fermi level<sup>4</sup> in magnetite is expected to benefit the injection of carrier spins into a given semiconductor.<sup>5</sup> For instance, magnetic tunnel transistors based on a Fe<sub>3</sub>O<sub>4</sub> emitter have demonstrated a high efficiency of spin-dependent hot electron transport by utilizing the high degree of spin polarization in the oxide material.<sup>6</sup>

We previously realized the growth of epitaxial Fe<sub>3</sub>O<sub>4</sub> films on GaAs(100) by combining the techniques of molecular beam epitaxy (MBE) and postgrowth annealing of Fe thin film under partial oxygen atmosphere.<sup>7-9</sup> These films show an in-plane uniaxial magnetic anisotropy (UMA) with an easy axis in the [0-11] direction of the GaAs(100) substrate, which is unexpected from a crystal symmetry perspective. In general, two distinctly different mechanisms, i.e., unidirectional interface bonding and anisotropic lattice relaxation, have been proposed to explain the UMA in hybrid ferromagnet/GaAs structures.<sup>10,11</sup> The latter effect only persists up to the relaxation length of the lattice constant. In contrast, magnetic anisotropy caused by anisotropic interface bonding is confined to the surface and is generally believed to occur due to the uniaxial nature of the Fe-Ga bonds at the

interfacial region. When these two arguments remain relevant in the case of Fe<sub>3</sub>O<sub>4</sub>/GaAs, it would be feasible to identify which of these two mechanisms is the dominant one by measuring the strength of the anisotropy as a function of the magnetic film thickness. In this work, we aim to correlate the observation of the UMA in the Fe<sub>3</sub>O<sub>4</sub>-based structures on GaAs to these two possible mechanisms using ferromagnetic resonance (FMR) measurements and detailed numerical simulations. Two specific systems are studied: Fe<sub>3</sub>O<sub>4</sub>/GaAs and Fe<sub>3</sub>O<sub>4</sub>/MgO/GaAs. The MgO tunneling barriers have already been used<sup>12</sup> to overcome the well-known conductivity mismatch between ferromagnetic metals and semiconductors in the diffusive regime.<sup>13</sup> Half-metallic Fe<sub>3</sub>O<sub>4</sub> with a MgO tunneling barrier<sup>14-16</sup> is therefore an intriguing hybrid structure for a highly efficient spin injector in semiconductors at room temperature.<sup>17,18</sup> The quality of the magnetite films fabricated by our approach was confirmed previously by a range of experimental techniques, including x-ray photoelectron spectroscopy, x-ray magnetic circular dichroism, reflection high-energy electron diffraction (RHEED), magneto-optical Kerr effect (MOKE), and superconducting quantum interference device magnetometry, as can be found elsewhere.<sup>19,20</sup> We find that in Fe<sub>3</sub>O<sub>4</sub>/GaAs the interfacial chemical bonding, rather than strain relaxation, is responsible for the presence of a UMA. The UMA has a distinctly different origin in Fe<sub>3</sub>O<sub>4</sub>/MgO/GaAs, where strain relaxation in the Fe<sub>3</sub>O<sub>4</sub> film dominates.

### II. EXPERIMENTAL DETAILS

Fe epitaxial films with a thickness spanning 3–8 nm were deposited in a vacuum MBE system with a base pressure of  $6 \times 10^{-9}$  mbar on GaAs(100) substrates at room temperature at a rate of 2 Å/min using electron-beam evaporation. Except for utilizing a higher oxygen partial pressure of  $8 \times 10^{-4}$  mbar for the 8-nm films, all other Fe films were then oxidized

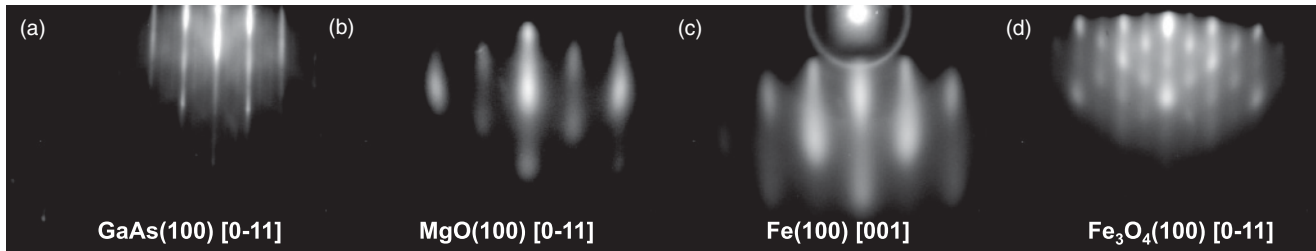


FIG. 1. RHEED patterns (a) GaAs(100) along [0-11], (b) MgO/GaAs, (c) Fe/MgO/GaAs, and (d) Fe<sub>3</sub>O<sub>4</sub>/MgO/GaAs.

at  $5 \times 10^{-5}$  mbar oxygen pressure for 180 s at 500 K to form the Fe<sub>3</sub>O<sub>4</sub> films, as described in our previous work.<sup>7,8</sup> A detailed discussion of the thickness regime of interest in this investigation is presented and elaborated upon in later paragraphs. The GaAs surface was flat and well crystallized, as evidenced by the RHEED pattern in Fig. 1(a). The thickness of the Fe layer before oxidation was monitored by an *in situ* microbalance.

Thin films of Fe<sub>3</sub>O<sub>4</sub> on top of MgO/GaAs(100) were grown using the same procedure as described above. Figure 1(b) shows the RHEED patterns of a 2.0-nm MgO layer epitaxially grown on a GaAs(100) surface. The pattern is streaky with several elongated spots, indicating the presence of some small crystalline islands on the smooth surface of the MgO film. This is attributed to the relatively large lattice mismatch (25.5%) between GaAs and MgO and an epitaxial relationship MgO(100)[001]//GaAs(100)[001], as deduced from Fig. 1(b). A 45° rotation of the Fe unit cell with respect to the MgO lattice is seen in Fig. 1(c), which results in a small lattice mismatch of 3.8% and an epitaxial relationship Fe(100)[011]//MgO(100)[001]. After annealing the Fe film in the oxygen environment, the typical RHEED pattern of Fe<sub>3</sub>O<sub>4</sub> is obtained, which is illustrated in Fig. 1(d). The magnetite cell is rotated back by 45° relative to the MgO lattice because such a configuration gives a nearly perfect lattice mismatch of  $\sim 0.33\%$ <sup>21,22</sup> with the MgO layer, and the overall epitaxial relationship is thus given as Fe<sub>3</sub>O<sub>4</sub>(100)[001]//MgO(100)[001]//GaAs(100)[001].

Magnetic hysteresis loops of the resulting Fe oxide films on GaAs(100) and MgO/GaAs(100) were measured by MOKE. The magnetic field was applied along the four major axes of the GaAs(100), i.e., [011], [001], [0-11], and [010]. The MOKE results revealed a clear magnetic anisotropy in both film stacks.

A UMA with an easy axis in the [0-11] direction was found in Fe<sub>3</sub>O<sub>4</sub>/GaAs, while the magnetic hard axis was in the [011] direction of the GaAs, as seen from Figs. 2(a)–2(p). For the thicker films, the UMA becomes weaker, while the cubic anisotropy becomes stronger with easy axes in (011) directions. In contrast with Fe<sub>3</sub>O<sub>4</sub>/GaAs, the UMA easy axis in Fe<sub>3</sub>O<sub>4</sub>/MgO/GaAs was found to be in the [011] direction and the hard axis was along [0-11]. Furthermore, from Figs. 2(q)–2(x), we can see that the UMA is drastically reduced after insertion of the MgO barrier, in addition to an increase of the cubic anisotropy.

So far, such a UMA has only been observed in our epitaxial Fe<sub>3</sub>O<sub>4</sub>/GaAs and Fe<sub>3</sub>O<sub>4</sub>/MgO/GaAs—not in similar structures grown by other techniques.<sup>23–25</sup> To further investigate the presence of a UMA, we extracted quantitative values for the

anisotropy constants from FMR and compared the surface and volume contributions to the anisotropy terms. The FMR measurements were performed at room temperature with a microwave frequency of 9.78 GHz using a Bruker electron spin resonance (model ER-200D-SRC). The resonance field data obtained from the measurement was fitted with theoretical curves derived from the Landau-Lifshitz equation without damping.<sup>26</sup> In general, at x-band frequencies such as 9.78 GHz, the small external static field required for the resonance condition may not be sufficient to magnetically saturate a given sample in all directions, thus leading to a large directional difference between the magnetization  $\mathbf{M}$  and the static field  $\mathbf{H}$ , which has been pointed out in earlier work.<sup>27</sup> Nevertheless, the external fields applied in our FMR measurement are sufficient to saturate the magnetization along the four crystallographic axes of the samples, which has been verified by the above MOKE loops. The approximation of a quiasignment of  $\mathbf{M}$  and  $\mathbf{H}$ , i.e.,  $\theta(\mathbf{M}, \mathbf{H}) = 0$ , can therefore be used to simplify the fitting equations in these directions.

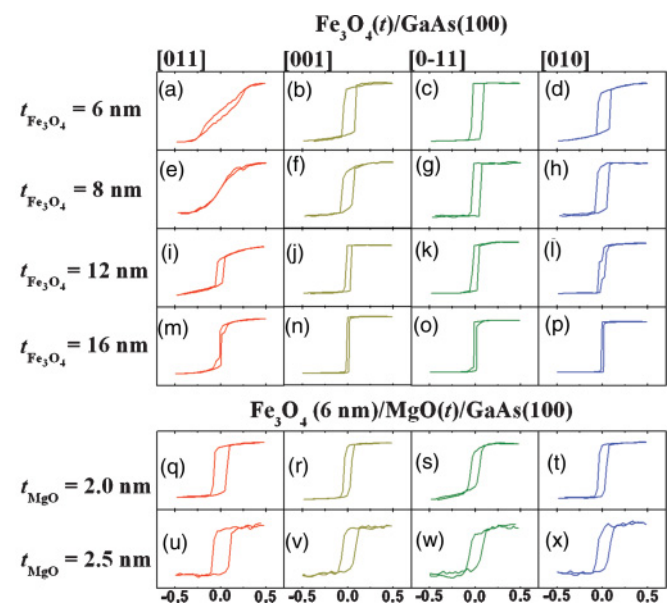


FIG. 2. (Color online) MOKE loops of (a)–(p) Fe<sub>3</sub>O<sub>4</sub>/GaAs(100) (upper panels) and (q)–(x) Fe<sub>3</sub>O<sub>4</sub>/MgO/GaAs(100) (lower panels). The external magnetic field direction is labeled above each column with respect to the GaAs(100) substrate. The horizontal axis gives the magnetic field ranging from  $-0.7$  to  $+0.7$  kOe, and the vertical axis gives the MOKE signal.

### III. ANISOTROPY CONSTANT AS A FUNCTION OF $\text{Fe}_3\text{O}_4$ THICKNESS IN $\text{Fe}_3\text{O}_4/\text{GAAS}$

The initial Fe epitaxial film thicknesses were chosen to be in the range of 3–8 nm for investigating the magnetic anisotropies of our  $\text{Fe}_3\text{O}_4$  films, based on our previous analysis: At a narrow thickness range  $\sim 1.6$  nm Fe, an S-shaped MOKE loop with zero hysteresis was observed, suggesting that the  $\text{Fe}_3\text{O}_4$  film after oxidation is superparamagnetic.<sup>7</sup> A good starting point is a Fe film thickness of 3 nm, in which case Fe is just fully oxidized and  $\text{Fe}_3\text{O}_4$  shows a ferromagnetic behavior after oxidation.<sup>18</sup> When the Fe thickness becomes  $> 8$  nm, the film will not be fully oxidized, resulting in a FeO or even Fe layer underneath  $\text{Fe}_3\text{O}_4$  near the interface.<sup>14,19</sup> After oxidation, the thickness of the  $\text{Fe}_3\text{O}_4$  film become twice the original Fe thickness, i.e.,  $t_{\text{Fe}_3\text{O}_4} = 6\text{--}16$  nm, as confirmed by atomic force microscopy and magnetization measurements.<sup>28</sup>

FMR measurements provide the magnetic-field direction dependence of the resonance field for varying  $\text{Fe}_3\text{O}_4$  thickness ( $t_{\text{Fe}_3\text{O}_4} = 6\text{--}16$  nm), as depicted in Fig. 3. It is evident that the  $\text{Fe}_3\text{O}_4(6\text{ nm})/\text{GaAs}$  film shows a dominant uniaxial symmetry,  $\sim \sin^2(\varphi_H)$ , with an easy axis along  $[0\text{-}11]$  ( $\varphi_H = 0^\circ$ ) and hard axis along  $[011]$  ( $\varphi_H = 90^\circ$ ), which are in good agreement with our previous work.<sup>8</sup> For  $t_{\text{Fe}_3\text{O}_4} \geq 8$  nm, fourfold cubic magnetocrystalline anisotropy starts to set in with the global hard axis still in the  $[011]$  direction of the GaAs; the  $[010]$  and  $[001]$  become equivalently magnetic easy directions, which is more pronounced in the thicker films.

The values of the cubic anisotropy constant  $K_1$  and UMA constant  $K_U$  were extracted from a theoretical fit of the resonance field data. The details for the theoretical fit were introduced in our previous paper.<sup>28</sup> The saturation magnetization used for data fitting is  $480\text{ emu/cm}^3$ , which is based on our previous work on the molecular magnetic moment of ultrathin  $\text{Fe}_3\text{O}_4$  films.<sup>29</sup> The moments of the  $\text{Fe}_3\text{O}_4$  films in the thickness range of 8–12 nm were found to be close to the bulk value of single-crystal magnetite. For the film thickness of 16 nm, we adopted a higher oxygen partial pressure during

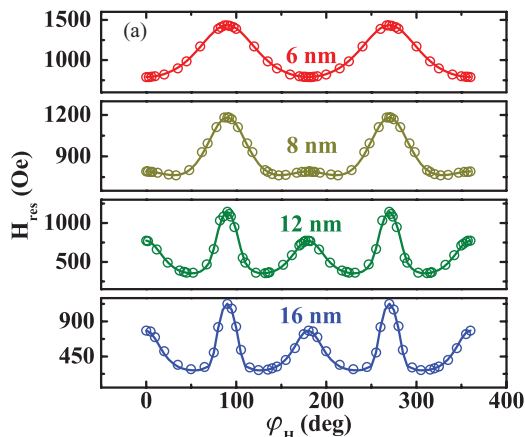


FIG. 3. (Color online) Angular dependence of the FMR field  $H_{\text{res}}$  for  $\text{Fe}_3\text{O}_4(6\text{--}16\text{ nm})/\text{GaAs}$ , where  $\varphi_H = 0^\circ, 45^\circ, 90^\circ$ , and  $135^\circ$  correspond, respectively, to the magnetic field applied along  $[0\text{-}11]$ ,  $[001]$ ,  $[011]$ , and  $[010]$  of the GaAs(100). The circles represent the experimental data, and the solid lines are theoretical fitted curves using the Landau-Lifshitz equation.

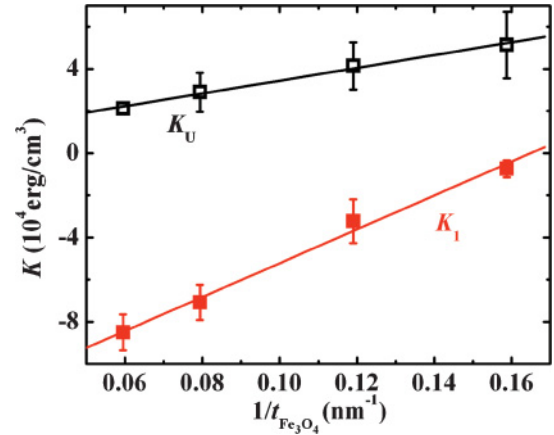


FIG. 4. (Color online) Thickness dependence of the cubic magnetic anisotropy ( $K_1$ ) and UMA ( $K_U$ ) of  $\text{Fe}_3\text{O}_4/\text{GaAs}(100)$ . The straight lines are linear fits to the data points.

the growth to prevent the presence of residual Fe found in Ref. 29. Figure 4 shows the values of  $K_1$  and  $K_U$  obtained for  $\text{Fe}_3\text{O}_4/\text{GaAs}$  as a function of the inverse  $\text{Fe}_3\text{O}_4$  thickness  $1/t_{\text{Fe}_3\text{O}_4}$ . The linear dependence of the anisotropy constants on the inverse  $\text{Fe}_3\text{O}_4$  thickness observed here is in good agreement with our previous analysis.<sup>8,30</sup> It is seen from Fig. 4 that the absolute value of the cubic anisotropy  $|K_1|$  dominates at higher coverage but is strongly reduced for thinner films. This can be interpreted as the long-range cubic order of the film lattice becoming better established with increased  $t_{\text{Fe}_3\text{O}_4}$ . In contrast, the uniaxial term  $K_U$  is largest for the thinnest film ( $t_{\text{Fe}_3\text{O}_4} = 6$  nm) and decreases with increasing  $t_{\text{Fe}_3\text{O}_4}$ , indicating that the UMA originates from the  $\text{Fe}_3\text{O}_4/\text{GaAs}$  interface. It is well known that Fe/GaAs shows a strong in-plane UMA, which is attributed to the interface bonding.<sup>31</sup> Compared to  $K_U \approx 10^5\text{ erg/cm}^3$  for Fe/GaAs,<sup>31–33</sup>  $K_U \approx 10^4\text{ erg/cm}^3$  for the  $\text{Fe}_3\text{O}_4/\text{GaAs}$  structure is almost an order of magnitude smaller, implying that the uniaxial nature of the Fe/Ga interface bonding is greatly reduced after oxidation.

Although  $K_1$  is an intrinsic property of the single-crystal epitaxial film, it is a function of the film thickness, as discussed by Bayreuther *et al.*<sup>34</sup> Here, we treat  $K_U$  and  $K_1$  as effective anisotropy constants; each is a combination of a volume and surface term, as suggested by Néel.<sup>35</sup> The surface term is the sum of the top and bottom surfaces, because experimentally these two contributions cannot be easily separated. Following Néel's phenomenological theory, the effective in-plane uniaxial and fourfold cubic anisotropy constants can be written as

$$K_U = K_{U,V} + \frac{K_{U,S}}{t} \quad (1a)$$

$$K_1 = K_{1,V} + \frac{K_{1,S}}{t}, \quad (1b)$$

where  $K_{U,V}$  and  $K_{U,S}$  are the volume and surface terms for  $K_U$ ,  $K_{1,V}$  and  $K_{1,S}$  are those for  $K_1$ , and  $t$  is equal to the  $\text{Fe}_3\text{O}_4$  thickness  $t_{\text{Fe}_3\text{O}_4}$ . The values in Fig. 4 scale almost linearly with  $1/t_{\text{Fe}_3\text{O}_4}$ , demonstrating that the change in the surface term with  $\text{Fe}_3\text{O}_4$  thickness is not significant. This implies that the surface contribution is constant (independent of the thickness)

TABLE I. Values of the surface and volume terms of the magnetic constants  $K_1$  and  $K_U$  for epitaxial  $\text{Fe}_3\text{O}_4/\text{GaAs}(100)$  obtained from a linear fit of the experimental data as a function of  $1/t_{\text{Fe}_3\text{O}_4}$ . The lower entries in the table give magnetic anisotropy constants taken from the literature, which have not been adjusted to remove the effect of the overlayer. For bulk  $\text{Fe}_3\text{O}_4$ ,  $K_{1,v} = K_1 = -11.8 \times 10^4 \text{ erg/cm}^3$ .

	$K_{1,v}$ ( $10^5 \text{ erg/cm}^3$ )	$K_{1,s}$ ( $10^{-2} \text{ erg/cm}^2$ )	$K_{U,v}$ ( $10^5 \text{ erg/cm}^3$ )	$K_{U,s}$ ( $10^{-2} \text{ erg/cm}^2$ )
$\text{Fe}_3\text{O}_4/\text{GaAs}$	$-1.33 \pm 0.06$	$8.04 \pm 0.52$	$0.04 \pm 0.02$	$3.03 \pm 0.19$
$\text{Cu/Fe/GaAs}$ <sup>32</sup>	$3.4 \pm 0.3$	$-1.2 \pm 0.4$	$-0.05 \pm 0.1$	$2.2 \pm 0.1$
$\text{Cu/Fe/GaAs}$ <sup>33</sup>	$4.6 \pm 0.3$	$-5.1 \pm 0.5$	–	$3.2 \pm 1.2$
$\text{Au/Fe/GaAs}$ <sup>31</sup>	$3.7 \pm 0.3$	$-3.2 \pm 0.5$	–	$10.0 \pm 1.0$

and that oxidation is almost uniform at the interface for various thicknesses. Linear fits performed on the two data sets in Fig. 4 for  $K_1$  and  $K_U$  as a function of  $1/t_{\text{Fe}_3\text{O}_4}$  give important values of the volume and surface contributions to  $K_1$  and  $K_U$ , as listed in Table I. Also included in the table are anisotropy constants for Fe/GaAs taken from the literature. These literature values have not been adjusted to remove the overlayer effects.<sup>36</sup>

As seen in Table I, the uniaxial volume term  $K_{U,v}$  is extremely small and practically zero, in accordance with the knowledge that  $K_{U,v} = 0$  for bulk  $\text{Fe}_3\text{O}_4$ . On the other hand, we can see that the UMA has a distinct interface origin, while the cubic anisotropy contains both the expected volume term  $K_{1,v}$  and a positive surface term  $K_{1,s}$ . The thickest film ( $t_{\text{Fe}_3\text{O}_4} = 16 \text{ nm}$ ) is predominantly fourfold, whereas the thinner films are mainly uniaxial.

In  $\text{Fe}_3\text{O}_4/\text{GaAs}$ ,  $K_{1,s}$  has a sign opposite the one in Fe/GaAs, caused by the negative sign of  $K_1$  in the former. This implies that the easy axes of  $K_1$  are rotated by  $45^\circ$  compared to those of Fe/GaAs. The value of  $K_{1,v}$  is slightly lower than expected for the bulk, indicating that even the thickest film studied here ( $t_{\text{Fe}_3\text{O}_4} = 16 \text{ nm}$ ) is not thick enough to recuperate entirely the bulklike magnetic anisotropy that, as we found from the fits, should occur at  $t_{\text{Fe}_3\text{O}_4} \approx 54 \text{ nm}$ .

The results confirm that interface bonding rather than strain relaxation plays a dominant role in causing the UMA in  $\text{Fe}_3\text{O}_4/\text{GaAs}$ , which is the same as in Fe/GaAs. However, given the substantially smaller surface term  $K_{U,s}$  in the former, the interface contribution to the UMA in  $\text{Fe}_3\text{O}_4/\text{GaAs}$  is believed to be weaker than that in Fe/GaAs. The reason for this is not yet known but might be related to the change in the uniaxial nature of the Fe-Ga bonds at the interface after oxidation.

#### IV. ANISOTROPY CONSTANTS AS A FUNCTION OF MGO THICKNESS IN $\text{Fe}_3\text{O}_4(6 \text{ nm})/\text{MGO}/\text{GAAS}$

We performed FMR measurements on  $\text{Fe}_3\text{O}_4(6 \text{ nm})/\text{MgO}/\text{GaAs}$  with varying MgO thickness to determine the magnetic anisotropy in such structures. Figure 5 illustrates the variation of the FMR field as a function of the in-plane orientation for  $\text{Fe}_3\text{O}_4$  films ( $t_{\text{Fe}_3\text{O}_4} = 6 \text{ nm}$ ) with varying MgO thickness ( $t_{\text{MgO}} = 0, 2.0, \text{ and } 2.5 \text{ nm}$ ). The  $\text{Fe}_3\text{O}_4/\text{GaAs}$  film in Fig. 5(a) shows a dominant uniaxial symmetry, as already pointed out in Sec. III. In contrast, Fig. 5(b) and 5(c) both show a global hard axis along  $[0-11]$  of the GaAs(100), indicating a  $90^\circ$  rotation of the UMA axes in  $\text{Fe}_3\text{O}_4/\text{MgO}/\text{GaAs}$  with respect to  $\text{Fe}_3\text{O}_4/\text{GaAs}$ . Figure 5(b) shows that for the  $\text{Fe}_3\text{O}_4$  film with  $t_{\text{MgO}} = 2.0 \text{ nm}$ , the angular dependence of the resonance field contains a small component of fourfold symmetry,  $\sim \sin^2(2\varphi_H)$ , superimposed on the UMA, indicating an in-plane cubic magnetocrystalline anisotropy coexisting with the UMA. Figure 5(c) shows a trend for the  $\text{Fe}_3\text{O}_4$  film with  $t_{\text{MgO}} = 2.5 \text{ nm}$  similar to that in Fig. 5(b) but with increased fourfold symmetry contribution due to stronger cubic anisotropy. These results have been quantified by theoretical fitting, resulting in the  $K_U$  and  $K_1$  values listed in Table II. The value of  $K_1$  increases after inserting the MgO barrier and continues to increase for thicker MgO layers. This reflects that, although the MgO film could be highly strained on top of GaAs due to the large lattice mismatch (25.5%), the strain in the  $\text{Fe}_3\text{O}_4$  film is still relaxed due to the nearly perfect lattice match between  $\text{Fe}_3\text{O}_4$  and MgO (0.33%).

Two important observations transpire from Table II: (1) the opposite signs of  $K_U$  for  $\text{Fe}_3\text{O}_4/\text{GaAs}(100)$  and  $\text{Fe}_3\text{O}_4/\text{MgO}/\text{GaAs}(100)$ , indicating a  $90^\circ$  rotation of the

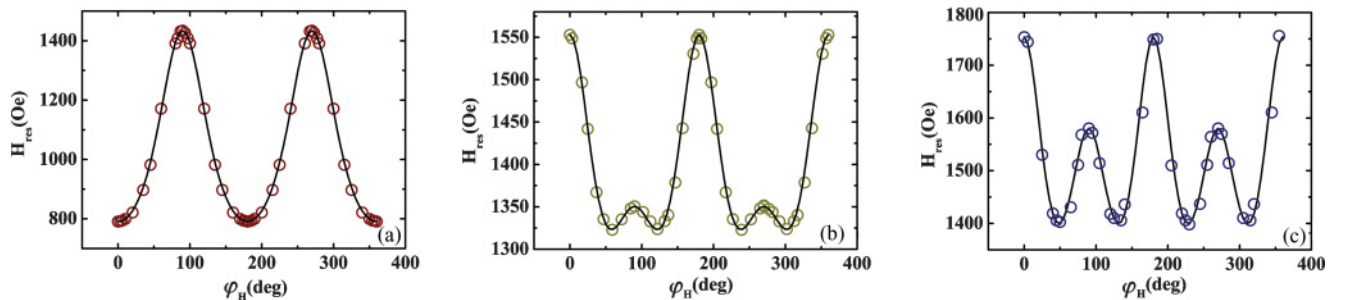


FIG. 5. (Color online) Angular dependence of the FMR field  $H_{\text{res}}$  for  $\text{Fe}_3\text{O}_4/\text{MgO}/\text{GaAs}$ , where  $\varphi_H = 0^\circ, 45^\circ, 90^\circ$ , and  $135^\circ$  correspond, respectively, to the magnetic field applied along  $[0-11]$ ,  $[001]$ ,  $[011]$ , and  $[010]$  of the GaAs(100). (a)  $\text{Fe}_3\text{O}_4(6 \text{ nm})/\text{GaAs}$ , (b)  $\text{Fe}_3\text{O}_4(6 \text{ nm})/\text{MgO}(2.0 \text{ nm})/\text{GaAs}$ , and (c)  $\text{Fe}_3\text{O}_4(6 \text{ nm})/\text{MgO}(2.5 \text{ nm})/\text{GaAs}$ . The dots represent the experimental data, and the solid lines are theoretical fitted curves.

TABLE II. Anisotropy constants for  $\text{Fe}_3\text{O}_4(6 \text{ nm})/\text{MgO}/\text{GaAs}(100)$  with varying MgO thickness  $t_{\text{MgO}}$  obtained from FMR.

$t_{\text{MgO}}$ (nm)	$K_1$ ( $10^4 \text{ erg/cm}^3$ )	$K_U$ ( $10^4 \text{ erg/cm}^3$ )
0	-0.49	4.05
2.0	-1.42	-1.32
2.5	-2.75	-0.86

magnetic axes of the UMA between both structures, and (2) the large decrease in magnitude of  $K_U$  in the  $\text{Fe}_3\text{O}_4/\text{MgO}/\text{GaAs}$  system with increasing MgO thickness. For  $t_{\text{MgO}} = 2.5 \text{ nm}$ ,  $K_U$  is strongly suppressed by a factor of 4.7. By comparing the 6-nm-thick  $\text{Fe}_3\text{O}_4$  film on GaAs with those of the same thickness on MgO/GaAs, where the former has a negligible cubic anisotropy but a *strong* in-plane UMA and the latter exhibits a dominant cubic anisotropy and a *weak* UMA, we can already see the following: (1) the interfacial contact between the GaAs substrate and the  $\text{Fe}_3\text{O}_4$  layer plays an important and direct role in causing the observed UMA in  $\text{Fe}_3\text{O}_4/\text{GaAs}$ , which is consistent with the conclusion drawn in Sec. III, and (2) the GaAs substrate underneath the MgO interlayer plays a crucial role in inducing the weak UMA in the case of  $\text{Fe}_3\text{O}_4/\text{MgO}/\text{GaAs}$ , which we explain next.

Although the presence of a UMA in  $\text{Fe}_3\text{O}_4/\text{MgO}/\text{GaAs}(100)$  seems surprising, the mechanism of interfacial uniaxial bonding can readily be ruled out because no in-plane UMA is observed for  $\text{Fe}_3\text{O}_4$  film grown on the MgO substrate.<sup>21,37-40</sup> Still, we believe that the GaAs substrate underneath the MgO plays a crucial role in inducing this unexpected anisotropy. Given the relatively large lattice mismatch between GaAs and MgO (25.5%), it is expected that

the MgO interlayer will be highly strained after deposition on the GaAs substrate. Combined with the extremely small lattice mismatch between  $\text{Fe}_3\text{O}_4$  and MgO (0.33%), a strain or strain-induced disorder mechanism originating from the MgO/GaAs interface is therefore one possible source for the UMA observed in  $\text{Fe}_3\text{O}_4/\text{MgO}/\text{GaAs}$ .

## V. CONCLUSIONS

The magnetic anisotropy constants of  $\text{Fe}_3\text{O}_4/\text{GaAs}$  and  $\text{Fe}_3\text{O}_4/\text{MgO}/\text{GaAs}(100)$  epitaxial spintronic structures were quantitatively determined using FMR measurements. From a linear fit of the anisotropy constants as a function of the inverse thickness of the magnetic film, the surface and volume contributions to both the cubic and the uniaxial anisotropies were distinguished. It was found that the unidirectional interface bonding rather than the strain effect is the main origin of the observed UMA in  $\text{Fe}_3\text{O}_4/\text{GaAs}$ . In contrast, in the  $\text{Fe}_3\text{O}_4/\text{MgO}/\text{GaAs}$  system, the magnetic easy axes of the UMA are rotated by  $90^\circ$  compared to  $\text{Fe}_3\text{O}_4/\text{GaAs}$ , along with a decrease in the magnitude of the UMA. The strain relaxation of the  $\text{Fe}_3\text{O}_4$  films is the mechanism responsible for the unexpected UMA in  $\text{Fe}_3\text{O}_4/\text{MgO}/\text{GaAs}$ , which is distinctively different from that in  $\text{Fe}_3\text{O}_4/\text{GaAs}$ .

Keeping in mind that strain relaxation may occur gradually as the film thickness is increased, leading to a UMA that is thickness dependent, those two preceding mechanisms are not necessarily easy to separate. Although the experimental results of this work are in good agreement with our proposed mechanisms, detailed structural information would be needed to provide further insight into the atomic scale origin of the UMA in such epitaxial  $\text{Fe}_3\text{O}_4$ -based hybrid structures on GaAs(100).

\*yx2@york.ac.uk

<sup>1</sup>J. J. Krebs, B. T. Jonker, and G. A. Prinz, *J. Appl. Phys.* **61**, 2596 (1987).

<sup>2</sup>P. K. J. Wong and Y. B. Xu, in *Spintronic Materials and Technology* (Taylor & Francis Group, New York & London, 2006), Chap. 15, pp. 337-370.

<sup>3</sup>M. L. Glasser and F. J. Milford, *Phys. Rev.* **130**, 1783 (1963).

<sup>4</sup>Y. S. Dedkov, U. Rudiger, and G. Guntherodt, *Phys. Rev. B* **65**, 064417 (2002).

<sup>5</sup>R. Mansell, J.-B. Laloe, S. N. Holmes, P. K. J. Wong, Y. B. Xu, I. Farrer, G. A. C. Jones, D. A. Ritchie, and C. H. W. Barnes, *J. Appl. Phys.* **108**, 034507 (2010).

<sup>6</sup>K. S. Yoon, J. Y. Yang, K. W. Kim, J. H. Koo, C. O. Kim, and J. P. Hong, *J. Appl. Phys.* **95**, 6933 (2004).

<sup>7</sup>Y. X. Lu, J. S. Claydon, Y. B. Xu, D. M. Schofield, and S. M. Thompson, *J. Appl. Phys.* **95**, 7228 (2004).

<sup>8</sup>Y. X. Lu, J. S. Claydon, Y. B. Xu, S. M. Thompson, K. Wilson, and G. van der Laan, *Phys. Rev. B* **70**, 233304 (2004).

<sup>9</sup>E. Liu, J. Z. Zhang, W. Zhang, P. K. J. Wong, L. Y. Lv, Y. Zhai, Y. B. Xu, and H. R. Zhai, *J. Appl. Phys.* **109**, 07C121 (2011).

<sup>10</sup>O. Thomas, Q. Shen, P. Schieffer, N. Tournerie, and B. Lepage, *Phys. Rev. Lett.* **90**, 017205 (2003).

<sup>11</sup>Y. B. Xu, D. J. Freeland, M. Tselepi, and J. A. C. Bland, *Phys. Rev. B* **62**, 1167 (2000).

<sup>12</sup>R. Wang, X. Jiang, R. M. Shelby, R. M. Macfarlane, S. S. P. Parkin, S. R. Bank, and J. S. Harris, *Appl. Phys. Lett.* **86**, 052901 (2005).

<sup>13</sup>G. Schmidt, D. Ferrand, L. W. Molenkamp, A. T. Filip, and B. J. van Wees, *Phys. Rev. B* **62**, R4790 (2000).

<sup>14</sup>X. W. Li, A. Gupta, G. Xiao, W. Qian, and V. P. Dravid, *Appl. Phys. Lett.* **73**, 3282 (1998).

<sup>15</sup>T. Kiyomura, M. Gomi, Y. Maruo, and H. Toyoshima, *IEEE Trans. Magn.* **35**, 3046 (1999).

<sup>16</sup>S. Kale, S. M. Bhagat, S. E. Lofland, T. Scabarozzi, S. B. Ogale, A. Orozco, S. R. Shinde, T. Venkatesan, B. Hannoyer, B. Mercey, and W. Prellier, *Phys. Rev. B* **64**, 205413 (2001).

<sup>17</sup>P. K. J. Wong, W. Zhang, and Y. B. Xu, *Phys. Stat. Solidi. A*, doi: 10.1002:psa.201084175 (to be published).

<sup>18</sup>P. K. J. Wong, W. Zhang, Y. B. Xu, S. Hassan, and S. M. Thompson, *IEEE Trans. Magn.* **44**, 2640 (2008).

<sup>19</sup>Y. X. Lu, J. S. Claydon, E. Ahmad, Y. B. Xu, S. M. Thompson, K. Wilson, and G. van der Laan, *IEEE Trans. Magn.* **41**, 2808 (2005).

- <sup>20</sup>P. K. J. Wong, W. Zhang, X. G. Cui, Y. B. Xu, J. Wu, Z. K. Tao, X. Li, Z. L. Xie, R. Zhang, and G. van der Laan, *Phys. Rev. B* **81**, 035419 (2010).
- <sup>21</sup>D. T. Margulies, F. T. Parker, F. E. Spada, R. S. Goldman, J. Li, R. Sinclair, and A. E. Berkowitz, *Phys. Rev. B* **53**, 9175 (1996).
- <sup>22</sup>T. Hibma, F. C. Voogt, L. Niesen, P. A. A. van der Heijden, W. J. M. de Jonge, J. J. T. M. Donkers, and P. J. van der Zaag, *J. Appl. Phys.* **85**, 5291 (1999).
- <sup>23</sup>M. Luysberg, R. G. S. Sofin, S. K. Arora, and I. V. Shvets, *Phys. Rev. B* **80**, 024111 (2009).
- <sup>24</sup>E. J. Preisler, J. Brooke, N. C. Oldham, and T. C. McGill, *J. Vac. Sci. Technol. B* **21**, 1745 (2003).
- <sup>25</sup>F. C. Voogt, T. Fujii, P. J. M. Smulders, L. Niesen, M. A. James, and T. Hibma, *Phys. Rev. B* **60**, 11193 (1999).
- <sup>26</sup>S. V. Vonsovskii, *Ferromagnetic Resonance* (Pergamon, London, 1966).
- <sup>27</sup>W. Wetzling, R. S. Smith, W. Jantz, and P. M. Ganser, *J. Magn. Magn. Mater.* **28**, 299 (1982).
- <sup>28</sup>Z. C. Huang, Y. Zhai, Y. X. Lu, G. D. Li, P. K. J. Wong, Y. B. Xu, Y. X. Xu, and H. R. Zhai, *Appl. Phys. Lett.* **92**, 113105 (2008).
- <sup>29</sup>Y. Zhai, L. Sun, Z. C. Huang, Y. X. Lu, G. D. Li, Q. Li, Y. B. Xu, J. Wu, and H. R. Zhai, *J. Appl. Phys.* **107**, 09B110 (2010).
- <sup>30</sup>Y. Zhai, Z. C. Huang, Y. Fu, C. Ni, Y. X. Lu, Y. B. Xu, J. Wu, and H. R. Zhai, *J. Appl. Phys.* **101**, 09D126 (2007).
- <sup>31</sup>S. McPhail, C. M. Gurtler, F. Montaigne, Y. B. Xu, M. Tselepi, and J. A. C. Bland, *Phys. Rev. B* **67**, 024409 (2003).
- <sup>32</sup>M. Madami, S. Tacchi, G. Carlotti, G. Gubbiotti, and R. L. Stamps, *Phys. Rev. B* **69**, 144408 (2004).
- <sup>33</sup>T. L. Monchesky, B. Heinrich, R. Urban, K. Myrtle, M. Klaua, and J. Kirschner, *Phys. Rev. B* **60**, 10242 (1999).
- <sup>34</sup>G. Bayreuther, M. Dumm, B. Uhl, R. Meier, and W. Kipferl, *J. Appl. Phys.* **93**, 8230 (2003).
- <sup>35</sup>L. Néel, *J. Phys. Radium.* **15**, 225 (1954).
- <sup>36</sup>P. K. J. Wong, Y. Fu, W. Zhang, Y. Zhai, Y. B. Xu, Z. C. Huang, Y. X. Xu, and H. R. Zhai, *IEEE. Trans. Magn.* **44**, 2907 (2008).
- <sup>37</sup>D. M. Lind, S. D. Berry, G. Chern, H. Mathias, and L. R. Testardi, *Phys. Rev. B* **45**, 1838 (1992).
- <sup>38</sup>W. Eerenstein, T. T. M. Palstra, T. Hibma, and S. Celotto, *Phys. Rev. B* **68**, 014428 (2003).
- <sup>39</sup>X. W. Li, A. Gupta, G. Xiao, and G. Q. Gong, *J. Appl. Phys.* **83**, 7049 (1998).
- <sup>40</sup>F. C. Voogt, T. T. M. Palstra, L. Niesen, O. C. Rogojuanu, M. A. Janes, and T. Hibma, *Phys. Rev. B* **57**, R8107 (1998).